Effects of Anthropogenic Emission Control and Meteorology þÿ Changes on the Inter-Annual Variations of PM2. Relationship in China

Qi, Ling

Multidisciplinary Digital Publishing Institute
2022-09-19

Qi, L.; Zheng, H.; Ding, D.; Wang, S. Effects of Anthropogenic Emission Control and þÿ Meteorology Changes on the Inter-Annual Variations of PM2.5 AOD Rel Remote Sens. 2022, 14, 4683.

http://hdl.handle.net/10138/349466

remote sensing

MDPI

Article

Effects of Anthropogenic Emission Control and Meteorology Changes on the Inter-Annual Variations of $PM_{2.5}$–AOD Relationship in China

Ling Qi [1], Haotian Zheng [2], Dian Ding [3] and Shuxiao Wang [2,4,*]

[1] School of Energy and Environmental Engineering, University of Science and Technology Beijing, Beijing 100083, China
[2] State Key Joint Laboratory of Environment Simulation and Pollution Control, School of Environment, Tsinghua University, Beijing 100084, China
[3] Institute for Atmospheric and Earth System Research (INAR)/Physics, Faculty of Science, University of Helsinki, 00014 Helsinki, Finland
[4] State Environmental Protection Key Laboratory of Sources and Control of Air Pollution Complex, Beijing 100084, China
* Correspondence: shxwang@tsinghua.edu.cn

Abstract: We identified controlling factors of the inter-annual variations of surface $PM_{2.5}$–aerosol optical depth (AOD) relationship in China from 2006 to 2017 using a nested 3D chemical transport model—GEOS-Chem. We separated the contributions from anthropogenic emission control and meteorological changes by fixing meteorology at the 2009 level and fixing anthropogenic emissions at the 2006 level, respectively. Both observations and model show significant downward trends of $PM_{2.5}$/AOD ratio (η, $p < 0.01$) in the North China Plain (NCP), the Yangtze River Delta (YRD) and the Pearl River Delta (PRD) in 2006–2017. The model suggests that the downward trends are mainly attributed to anthropogenic emission control. $PM_{2.5}$ concentration reduces faster at the surface than aloft due to the closeness of surface $PM_{2.5}$ to emission sources. The Pearson correlation coefficient of surface $PM_{2.5}$ and AOD ($r_{PM\text{-}AOD}$) shows strong inter-annual variations (±27%) but no statistically significant trends in the three regions. The inter-annual variations of $r_{PM\text{-}AOD}$ are mainly determined by meteorology changes. Except for the well-known effects from relative humidity, planetary boundary layer height and wind speed, we find that temperature, tropopause pressure, surface pressure and atmospheric instability are also important meteorological elements that have a strong correlation with inter-annual variations of $r_{PM\text{-}AOD}$ in different seasons. This study suggests that as the $PM_{2.5}$–AOD relationship weakens with reduction of anthropogenic emissions, validity of future retrieval of surface $PM_{2.5}$ using satellite AOD should be carefully evaluated.

Keywords: $PM_{2.5}$–AOD relationship; inter-annual variations; anthropogenic emission control; meteorology changes

Citation: Qi, L.; Zheng, H.; Ding, D.; Wang, S. Effects of Anthropogenic Emission Control and Meteorology Changes on the Inter-Annual Variations of $PM_{2.5}$–AOD Relationship in China. *Remote Sens.* **2022**, *14*, 4683. https://doi.org/10.3390/rs14184683

Academic Editor: Simone Lolli

Received: 10 August 2022
Accepted: 15 September 2022
Published: 19 September 2022

1. Introduction

Long-term exposure to ambient fine particles ($PM_{2.5}$) in China causes more than 1 million early deaths every year [1,2]. To protect human health, it is critical to evaluate human exposure using high-resolution surface $PM_{2.5}$ data. However, nationwide surface in situ measurements of $PM_{2.5}$ were sparse and unavailable until 2013. Thus, studies usually retrieve surface $PM_{2.5}$ with horizontal resolution of 1–10 km using satellite aerosol optical depth (AOD) with large spatial and temporal coverage [3–6].

Accurate retrieval of surface $PM_{2.5}$ from satellite AOD requires a strong $PM_{2.5}$–AOD relationship [7]. Studies use $PM_{2.5}$/AOD ratio (η) and linear correlation coefficient of $PM_{2.5}$ and AOD ($r_{PM\text{-}AOD}$) to quantify the $PM_{2.5}$–AOD relationship. Wang [8] explored the correlation between AOD from Moderate Resolution Imaging Spectroradiometer (MODIS)

and hourly surface $PM_{2.5}$ measurements in Jefferson county, Alabama, and showed a strong correlation ($r_{PM\text{-}AOD}$ = 0.7) for daily average and even stronger correlation for a monthly mean ($r_{PM\text{-}AOD}$ > 0.9). Strong correlations were also observed in Beijing ($r_{PM\text{-}AOD}$ = 0.79) [9] and at background sites in the North China Plain (NCP) [10] and in Nanjing in the Yangtze River Delta (YRD) [11] in China. However, nationwide studies [7,12] showed large spatial variations of $r_{PM\text{-}AOD}$ in 368 cities across China (0.01 < $r_{PM\text{-}AOD}$ < 0.88) in 2013–2017. Specifically, the $r_{PM\text{-}AOD}$ value is high in central China and relatively lower in eastern coastal regions and western arid regions [12,13]. Similar results were found using AOD products with a finer spatiotemporal resolution, such as advanced Himawari-8 imager AOD with hourly resolution and 5 km horizontal resolution [14] and multi-angle implementation of atmospheric correction (MAIAC) with 1 km horizontal resolution [15].

Aerosol type, meteorology and topography are important elements that affect the $PM_{2.5}$–AOD relationship. Observations in Beijing showed that η is smaller for scattering-dominant coarse-mode aerosols than for absorbing-dominant fine-mode aerosols [9]. A stronger correlation for the scattering-dominated aerosols was also found based on observations across 368 cities in China [14]. Observations in Nanjing showed that $r_{PM\text{-}AOD}$ is larger for aerosols with larger Angstrom exponent [11]. Meteorological elements, such as relative humidity (RH), planetary boundary layer height (PBLH) and wind speed, are critical factors that affect the $PM_{2.5}$–AOD relationship. The higher the RH, wind speed and PBLH, the smaller the η [9]. Using RH corrections improves surface PM_{10} estimates from satellite AOD in Beijing [16]. Including vertical correction via PBLH increases $r_{PM\text{-}AOD}$ in northwestern China [17]. However, nationwide studies [9,15] suggest that correction by RH and PBLH does not necessarily increase $r_{PM\text{-}AOD}$. $r_{PM\text{-}AOD}$ decreases in a few regions in different seasons. For topography, the $PM_{2.5}$–AOD relationship is stronger in basin areas and is weaker over plateaus [12,14,15].

Most current studies focus on spatiotemporal variations of the $PM_{2.5}$–AOD relationship in recent years, but studies on decadal trends are rare. In addition, most studies are observation-based, and thus it is difficult to separate contributions from different factors. Due to the tough clean air policies, anthropogenic emissions of SO_2 in China have declined markedly since 2006, and NOx emissions have reduced strongly after 2011, particularly after 2013 [18]. However, in 2006–2017, biomass burning emissions showed no statistically significant trends [19]. In addition, annual total biomass burning emissions of NMVOCs, NOx, NH_3, SO_2, BC, OC and primary $PM_{2.5}$ only account for 1–8% of the total emissions [18,19]. The objective of this work is to systematically quantify the relative contributions of anthropogenic emission control and meteorology changes to trends and the inter-annual variations of the $PM_{2.5}$–AOD relationship in China in 2006–2017. We use a nested global 3D chemical transport model—GEOS-Chem—to simulate the $PM_{2.5}$–AOD relationship in China. We separate the contribution from anthropogenic emissions and meteorology changes by fixing meteorology at the 2009 level and fixing anthropogenic emissions at the 2006 level, respectively. We investigate responses of the $PM_{2.5}$–AOD relationship to anthropogenic emission changes and identify major meteorological elements that influence the inter-annual variations of the $PM_{2.5}$–AOD link.

2. Materials and Methods

2.1. Observations

We used MODIS Collection 6.1 Level-3 daily mean Dark Target and Deep Blue combined AOD data at 550 nm (https://modis-atmos.gsfc.nasa.gov/MOD08_M3/index.html, accessed on 16 June 2021). Collection 6.1 modified aerosol retrieval over the land surface when urban percentage is larger than 20% using a revised surface characterization and improved surface modeling in elevated terrain (Collection 6.1 Change Document). On a global scale, the expected errors are ± (0.05 + 15%) over land for Dark Target retrievals at the 10-km spatial resolution, ± (0.03 + 21%) for arid path retrievals and ± (0.03 + 18%) for vegetated path retrievals for Deep Blue retrievals. On regional scale, 60–83% of MODIS

C6.1 AOD data are within range of ± (0.05 + 15%) in NCP [20] and 90% of MODIS C5 data fall in the range of ± (0.05 + 20%) in YRD [21]. See details in reference [22].

We used surface in situ measurements of $PM_{2.5}$ from the China Ministry of Ecology and Environment network (https://www.mee.gov.cn, accessed on 16 June 2021) with 484 sites in 2013, 670 sites in 2014 and 1498 sites in 2015–2017 (Figure 1). $PM_{2.5}$ concentrations were determined by two methods: Thermo Scientific Continuous Ambient Particle Monitor TEOM-FDMS (Waltham, MA, USA) (about 60% of the sites) and β-gauge (the remaining 40% of the sites) with quality control (National Ambient Air Quality Standards, GB3095-2012; available at: http://english.mee.gov.cn/Resources/standards/Air_Environment/quality_standard1/201605/t20160511_337502.shtml, accessed on 16 June 2021). $PM_{2.5}$ concentrations determined by the two methods are highly correlated (r^2 = 0.95), but the concentrations measured by TEOM equipment are 15–23% lower than those measured by β-gauge [23]. Since the measurement method used at each site was unavailable, we used available data from all sites by the two methods, bringing uncertainties to the analysis.

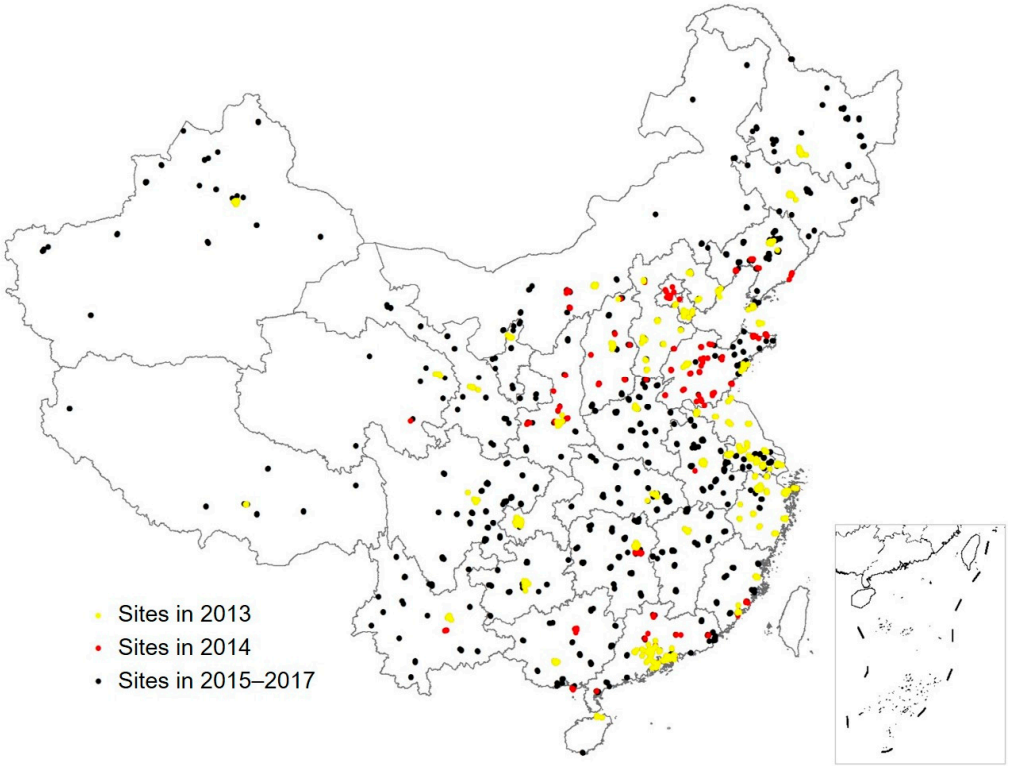

Figure 1. In situ surface $PM_{2.5}$ measurement sites in 2013 (yellow circles), 2014 (red circles) and 2015–2017 (black circles) used in this study.

2.2. Model Description

We use the 3D chemical transport model, GEOS-Chem version 11.01, to simulate surface $PM_{2.5}$ and AOD in China. We use a nested model with a horizontal resolution of 0.5° latitude × 0.667° longitude over Asia and the boundary conditions were archived from global simulations at 2° latitude × 2.5° longitude (see model grids at http://wiki.seas.harvard.edu/geos-chem/index.php/GEOS-Chem_horizontal_grids, accessed on 29 August 2022). Meteorological fields are from Modern-Era Retrospective analysis for Research and Application, Version 2 (MERRA-2). We ran the model with full gaseous chemistry and online aerosol calculations. GEOS-Chem simulates the thermodynamics of aerosols using the ISORROPIA II package [24]. The model couples aerosol and gas-phase chemistry through nitrate and ammonium partitioning [25], sulfur chemistry in clouds and aerosols [26], secondary organic aerosol formation [27,28] and uptake of acidic gases by sea salt and dust [29]. Monthly anthropogenic emissions of SO_2, NOx, BC, OC, NMVOCs and NH_3 in Asia are from the multi-resolution emission inventory developed by Tsinghua

University (Available at: http://meicmodel.org/, accessed on 29 August 2022) [18]. We updated anthropogenic emission inventories of these species in China in 2006–2017 [30]. Daily open biomass burning emissions are from the Global Fire Emissions Database, Version 4 (Available at: https://daac.ornl.gov/VEGETATION/guides/fire_emissions_v4_R1.html, accessed on 29 August 2022) [31] with horizontal resolution of 0.25° latitude × 0.25° longitude. Dry and wet removal of aerosols follow [32] and [33], respectively. The model simulation of AOD, surface $PM_{2.5}$ and its components are extensively validated against in situ station radiometer AOD measurements, MODIS AOD, surface in situ measurements of $PM_{2.5}$ and its components in previous studies [22,34].

2.3. Experimental Setup

We performed three experiments to quantify the contributions of anthropogenic emission control and meteorology changes to the $PM_{2.5}$–AOD relationship in China. In the BASE experiment, $PM_{2.5}$ and AOD were simulated with varying anthropogenic emissions and meteorological fields in each year from 2006 to 2017. In the FIXEMISS experiment, anthropogenic emissions were fixed at the 2006 level, when China started to control SO_2 emissions [35]. The variations in this experiment reflect the effects of meteorology changes in 2006–2017. In the FIXMET experiment, the meteorological field was fixed at the 2009 level in each year in 2006–2017. We selected 2009 because the annual mean $PM_{2.5}$ concentration in 2009 was the closest to the 12-year average. The variations in this experiment reflect the effects of anthropogenic emission control.

We analyze results in three key regions in China: the NCP (35–41°N, 110–120°E), the YRD (27–35°N, 116–122°E) and the Pearl River Delta (PRD, 22–25°N, 110–117°E). See details of the regions in reference [22]. $PM_{2.5}$/AOD ratio η and Pearson correlation coefficient $r_{\text{PM-AOD}}$ were proved to be good parameters to quantify the $PM_{2.5}$–AOD relationship [6,12,13,36]. The former is a conversion factor [37] and indicates the dry mass $PM_{2.5}$ concentration per unit aerosol optical thickness. The latter indicates the strength and direction of the linear relationship between surface dry mass $PM_{2.5}$ and AOD. A previous study showed that stronger $PM_{2.5}$–AOD relationship produces better surface $PM_{2.5}$ retrieval [12]. We archived daily mean $PM_{2.5}$ concentration and AOD data from GEOS-Chem runs in the three experiments. We estimated the daily η (η = $PM_{2.5}$_daily/AOD_daily) in each model grid first and then estimated the monthly, seasonal and annual mean in each region. We estimated $r_{\text{PM-AOD}}$ using daily mean $PM_{2.5}$ and AOD in each model grid in each month, season and year and then estimated the mean value in each region.

3. Results

3.1. Observed and Simulated Long-Term Trends of $PM_{2.5}$–AOD Relationship

Observations show that the ratios of η observed at the in situ sites in 2013–2017 vary with seasons. The largest η is in winter (114–212 μg m^{-3}) and the smallest in summer (44–61 μg m^{-3}, Figure 2). This is possibly explained by several reasons. First, anthropogenic emissions in winter are 30% larger than those in summer in NCP, while the differences in YRD and PRD are within 8%. Thus, the ratio in NCP in winter is higher than those in other seasons and regions. Second, stable stratification in winter confined surface emissions to the boundary layer and enhances surface $PM_{2.5}$ concentration. Simulated surface $PM_{2.5}$ concentration in winter is consistently 16–54% larger than those in summer in the three regions. Third, aerosol loading in NCP in summer is 25–43% larger than that in winter. In YRD and PRD, aerosol loading in summer is also smaller than that in winter, but the difference is smaller than those of surface $PM_{2.5}$ concentrations. Fourth, the simulated hygroscopic factors of different species in summer are 1–45% larger than those in winter, enhancing AOD in summer.

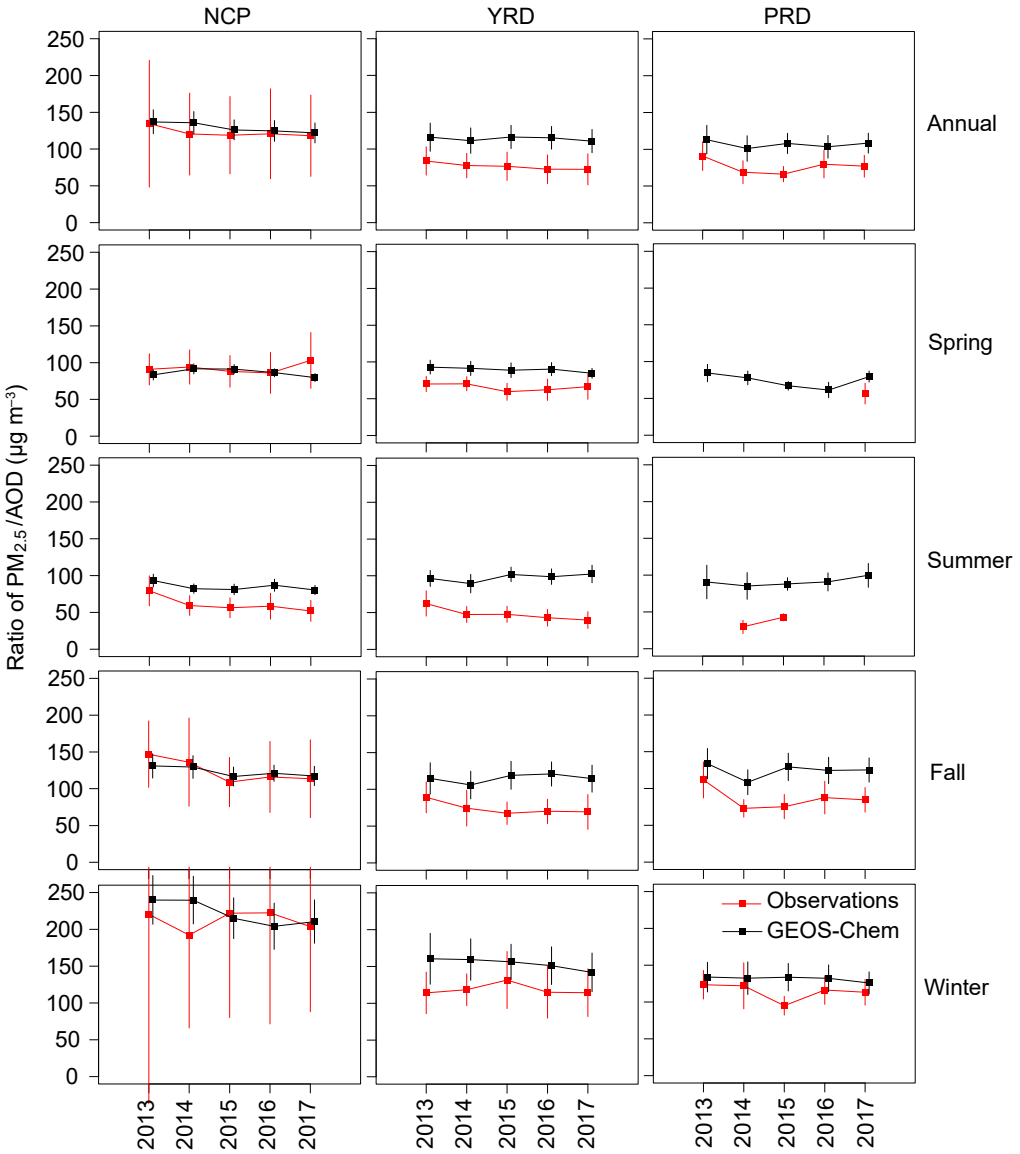

Figure 2. Observed (red lines) and GEOS-Chem simulated (black lines) ratio of $PM_{2.5}$/AOD (η) in NCP, YRD and PRD in 2013–2017. The bars are standard deviations.

GEOS-Chem overestimates η by 24–63% in NCP, YRD and PRD due to the overestimate of surface $PM_{2.5}$ and underestimate of AOD [22]. Observations show that annual mean ratios of η are decreasing at rates of −2.6, −3.6 and −2.1% year^{-1} in NCP (p-value = 0.13), YRD (p-value = 0.02) and PRD (p-value = 0.67) in 2013–2017, with the fastest decline in summer (−9.1, −10.3 and −2.6% year^{-1}) and followed by those in fall (−7.0, −5.9 and −4.6% year^{-1}). In 2006–2017, the simulated η show significant decreasing rates of −1.2, −0.7 and −1.4% year^{-1} in NCP, YRD and PRD (p-value < 0.01), respectively. Different from trends of AOD and surface $PM_{2.5}$ [22], the difference of reduction rates of η before and after 2013 are much smaller (Figure 3). Specifically, the simulated reduction rates of η in 2013–2017 are smaller than those in 2006–2013 by 16% in NCP, but the rates in YRD and PRD in 2013–2017 are 11% and 100% larger than those in 2006–2013.

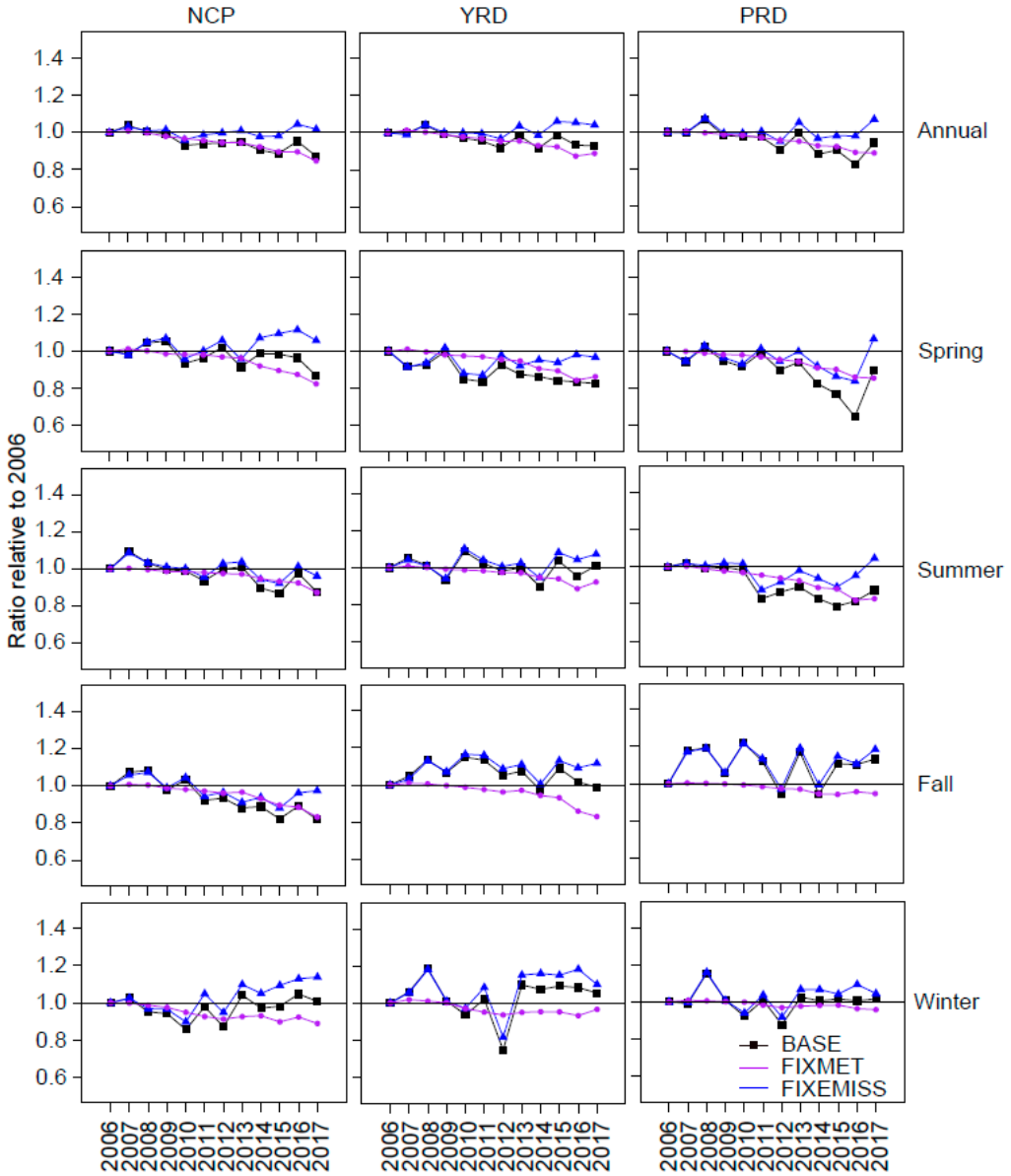

Figure 3. $PM_{2.5}$/AOD ratios (η) relative to their values in 2006 in GEOS-Chem simulations in 2006–2017. Three experiments are shown: varying meteorology and varying emissions (BASE, black lines), varying anthropogenic emissions with meteorological fields fixed at the 2009 level (FIXMET, purple lines), varying meteorological fields with fixed anthropogenic emissions at the 2006 level (FIXEMISS, blue lines).

Observations show that $r_{\text{PM-AOD}}$ in 2013–2017 is decreasing in the three key regions, but the trends are statistically insignificant (p-value > 0.76). These trends are in general agreement with recent studies [12]. GEOS-Chem reproduces the inter-annual variations of $r_{\text{PM-AOD}}$ with a bias of −33–222% (Figure 4). The model overestimates $r_{\text{PM-AOD}}$ for the annual mean and in spring-fall. The overestimate is possibly because the model does not resolve AOD from coarse particles. In contrast, the model underestimates $r_{\text{PM-AOD}}$ in winter, possibly due to the overestimated isolation of the boundary layer by the model [22]. $r_{\text{PM-AOD}}$ shows no significant trends in the three key regions in 2006–2017, but the inter-annual variations are substantial (Figure 5). The $r_{\text{PM-AOD}}$ values vary by ±27% in the 12 years in spring–fall. In winter, $r_{\text{PM-AOD}}$ varies between −0.47 and 0.38.

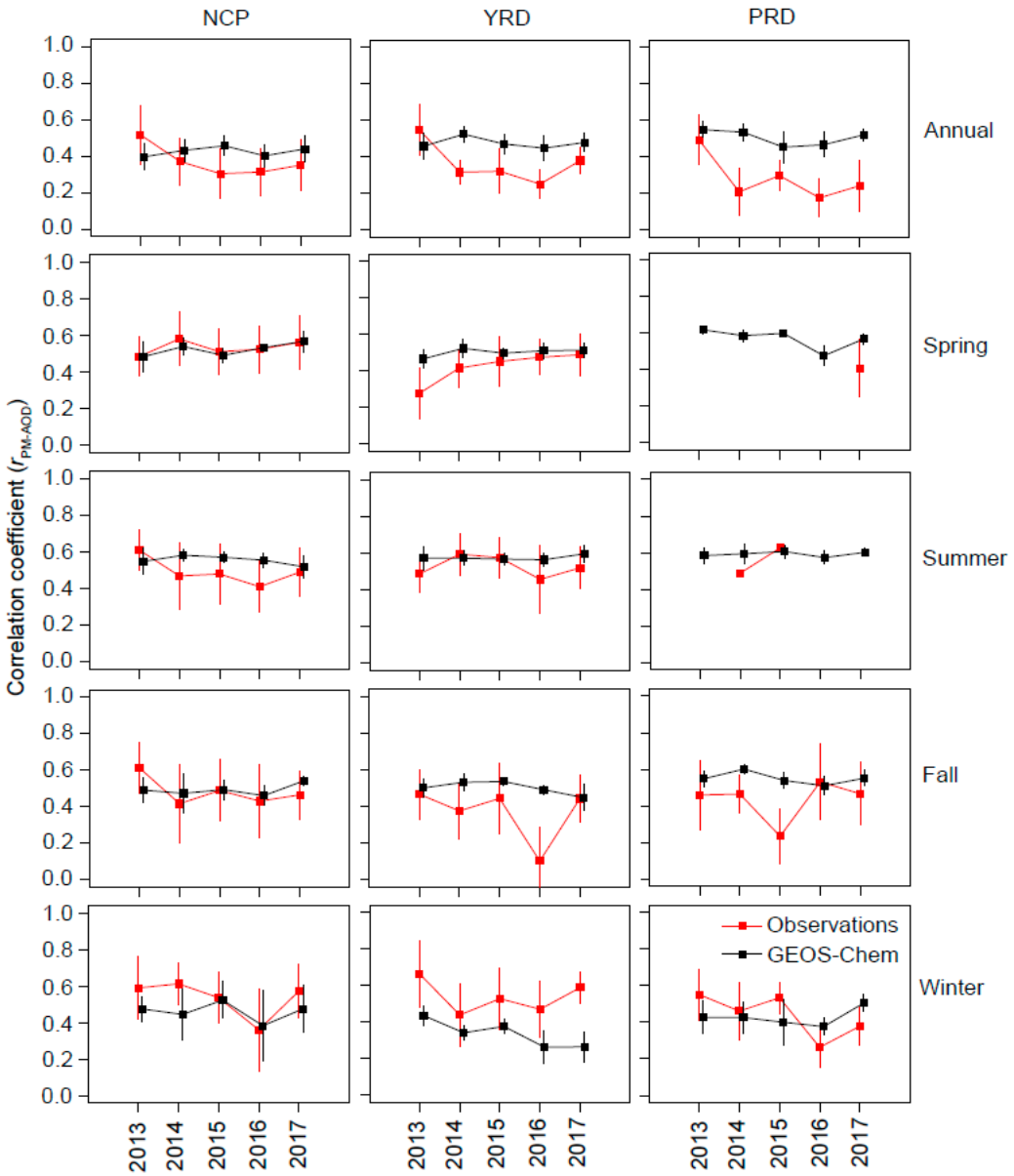

Figure 4. Observed (red lines) and GEOS-Chem simulated (black lines) annual and seasonal mean correlation coefficients of daily $PM_{2.5}$ and daily AOD ($r_{PM\text{-}AOD}$) in NCP, YRD and PRD in 2013–2017. The bars are standard deviations.

3.2. Contributions of Anthropogenic Emission Control and Meteorology Changes to $PM_{2.5}$–AOD Relationship

The decrease of η in 2006–2017 is mainly attributed to anthropogenic emission changes (Table 1). Specifically, meteorology changes tend to increase η in NCP and YRD, but contribute 10% to the reduction of η in PRD in FIXMET. In addition, η in BASE correlate stronger with η in FIXMET ($0.70 < r < 0.87$) than those in FIXEMISS ($0.26 < r < 0.64$). The downward trends of surface $PM_{2.5}$ and AOD in recent years are also attributed to anthropogenic emission changes [38,39]. GEOS-Chem suggests that the annual mean surface $PM_{2.5}$ decreases faster than AOD by 68% in NCP, 59% in YRD and 72% in PRD in 2006–2017 in FIXMET.

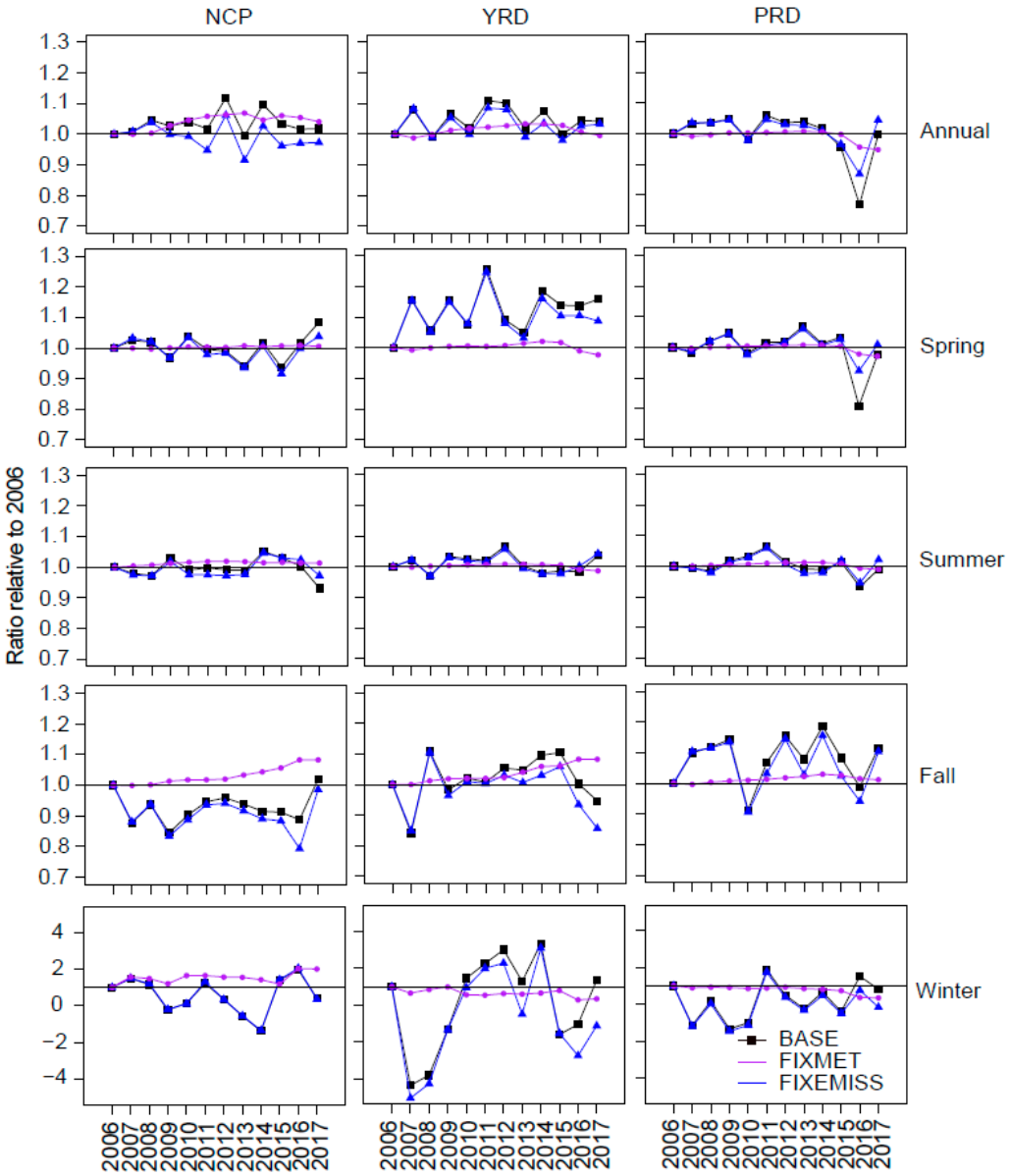

Figure 5. Annual and seasonal mean correlation coefficient of daily $PM_{2.5}$ and daily AOD ($r_{PM\text{-}AOD}$) relative to their values in 2006 in GEOS-Chem simulations in 2006–2017. Three experiments are shown: varying meteorology and varying emissions (BASE, black lines), varying anthropogenic emissions with meteorological fields fixed at the 2009 level (FIXMET, purple lines), varying meteorological fields with fixed anthropogenic emissions at the 2006 level (FIXEMISS, blue lines).

On a seasonal scale, the downward trends of η (BASE) are also attributed to anthropogenic emission reductions (Table 1). The downward trends of η in FIXMET are statistically significant in the four seasons. Meteorology changes increase η in spring and winter, but decrease η in summer and fall in NCP, and show limited effects on trends of η in other regions. In FIXMET in NCP, AOD decreases at the rate of 0.8% year^{-1} in spring, but surface $PM_{2.5}$ shows no trends; thus, η increases. The inter-annual variations of AOD in this region are controlled by temperature and vertical air movement at 850 hPa and surface RH [22]. However, none of these meteorological elements showed statistically significant trends over the 12 years. The weakening of the East Asian summer monsoon enhances aerosol concentrations but AOD increase (0.9% year^{-1}) faster than surface $PM_{2.5}$ (0.1% year^{-1}), producing a negative trend of η. Similar upward trends are observed for fall (AOD: 1.4% year^{-1} (p-value < 0.1); surface $PM_{2.5}$: 0.3% year^{-1}). The strong enhancement of

AOD is related to the decreased potential vorticity (−0.02 PVU year^{-1}, p-value < 0.05) and the increased RH at 850 hPa (0.002 year^{-1}). In winter, AOD decreases significantly over the 12 years (−1.2% year^{-1}, p-value < 0.01), but surface $PM_{2.5}$ increases; thus, η increases. The strong decrease of AOD is attributed to the significant increase of northerly wind speed at 850 hPa (0.15 m s^{-1} year^{-1}, p-value < 0.1). The inter-annual variations of η are also strongly affected by meteorology changes on the seasonal scale. H in BASE correlate stronger with η in FIXEMISS than those in FIXMET in fall and winter in the three regions (Table 2).

Table 1. GEOS-Chem simulated trends of $PM_{2.5}$/AOD ratios (η, μg m^{-3} year^{-1}) in 2006–2017 in NCP, YRD and PRD.

Season	Experiments	NCP	YRD	PRD
Annual	BASE	−1.25 *	−0.76 $^{+}$	−1.40 *
	FIXEMISS	0.04	0.41	−0.03
	FIXMET	−1.39 *	−1.25 *	−1.16 *
Spring	BASE	−0.87 $^{\#}$	−1.48 *	−2.41 *
	FIXEMISS	0.75 $^{\#}$	0.06	−0.54
	FIXMET	−1.59 *	−1.56 *	−1.46 *
Summer	BASE	−1.42 *	−0.38	−2.22 *
	FIXEMISS	−0.70 $^{\#}$	0.37	−0.49
	FIXMET	−1.01 *	−0.96 *	−1.83 *
Fall	BASE	−2.36 *	−0.50	−0.22
	FIXEMISS	−1.11 $^{+}$	0.41	0.18
	FIXMET	−1.48 *	−1.49 *	−0.64 *
Winter	BASE	0.39	0.23	−0.17
	FIXEMISS	1.45 $^{+}$	0.99	0.37
	FIXMET	−1.06 *	−0.68 *	−0.43 *

$^{\#}$ significant at 90% level (0.05 < p < 0.1); $^{+}$ significant at 95% level (0.01 < p < 0.05); * significant at 99% level (p < 0.01).

Table 2. Correlation coefficients of $PM_{2.5}$/AOD (η) in the BASE experiment with those in FIXEMISS and FIXMET.

Season	Experiments	NCP	YRD	PRD
Annual	FIXEMISS	0.42	0.26	0.64
	FIXMET	0.87	0.70	0.77
Spring	FIXEMISS	0.30	0.57	0.81
	FIXMET	0.58	0.68	0.78
Summer	FIXEMISS	0.95	0.83	0.76
	FIXMET	0.76	0.35	0.79
Fall	FIXEMISS	0.89	0.77	0.97
	FIXMET	0.85	0.50	0.28
Winter	FIXEMISS	0.83	0.94	0.92
	FIXMET	0.00	0.30	0.26

Meteorology changes show larger effects on inter-annual variations of $r_{PM\text{-}AOD}$ than anthropogenic emission control in 2006–2017 (Figure 5). In the FIXMET experiment, $r_{PM\text{-}AOD}$ increase significantly in 2006–2013 (p-value < 0.01) and decrease in 2013–2017 (p-value = 0.20 in NCP, 0.02 in YRD and PRD). In contrast, no significant trends are seen in FIXEMISS. Combining the effects of anthropogenic emission changes and meteorology changes in the BASE experiment, the trends of $r_{PM\text{-}AOD}$ are statistically insignificant, indicating that meteorology changes have larger influences on $r_{PM\text{-}AOD}$ than anthropogenic emission changes in 2006–2017. In addition, $r_{PM\text{-}AOD}$ in BASE correlates stronger to $r_{PM\text{-}AOD}$ in FIXEMISS (0.73 < r < 0.95) than those in FIXMET (0.17 < r < 0.63, Table 3). Moreover, the inter-annual variations of annual $r_{PM\text{-}AOD}$ caused by meteorology changes (−14%–+7%)

are much larger than those caused by anthropogenic emission changes (−5%–+3%). On the seasonal scale, $r_{PM\text{-}AOD}$ in BASE also correlate stronger to $r_{PM\text{-}AOD}$ in FIXEMISS than those in FIXMET, similar to the comparison on the annual scale (Table 3).

Table 3. Correlation coefficients of $r_{PM\text{-}AOD}$ in the BASE experiment with those in FIXEMISS and FIXMET.

Season	Experiments	NCP	YRD	PRD
Annual	FIXEMISS	0.73	0.95	0.96
	FIXMET	0.26	0.17	0.63
Spring	FIXEMISS	0.94	0.95	0.94
	FIXMET	−0.18	−0.04	0.69
Summer	FIXEMISS	0.82	0.96	0.92
	FIXMET	0.14	0.06	0.53
Fall	FIXEMISS	0.90	0.91	0.96
	FIXMET	0.15	0.21	0.28
Winter	FIXEMISS	0.99	0.95	0.96
	FIXMET	−0.18	0.26	0.36

3.3. Responses of $PM_{2.5}$ /AOD Ratios to Anthropogenic Emission Changes (FIXMET)

AOD is determined by both aerosol loading and the hygroscopic growth factor from the surface to the top of the atmosphere ([22], Section 2.1). GEOS-Chem shows that in FIXMET the hygroscopic growth factors do not change over the years, and the decrease of η in 2006–2017 is mainly due to faster decrease of $PM_{2.5}$ at the surface than aloft (Figure 6). We estimate the reduction rates of $PM_{2.5}$ in 2006–2017 (($PM_{2.5\_2017}$–$PM_{2.5\_2006}$)/$PM_{2.5\_2006}$) at various heights from the surface to 500 hPa. The reduction rates of $PM_{2.5}$ at 800 hPa (500 hPa) are 7% (48%), 5% (47%) and 20% (55%) smaller than those at the surface in NCP, YRD and PRD, respectively. The largest difference in reduction rates between the surface and aloft is from OA and the ratio decreases with increasing altitude monotonically. In contrast, the reduction rate of sulfate-nitrate-ammonium (SNA) increases slightly below 800 hPa in NCP and YRD (Figure 6, see model validation of $PM_{2.5}$ components in [22,34]).

GEOS-Chem shows that reduction rates of OA in surface $PM_{2.5}$ are slightly larger than those of AOD_{OA} in winter (<25%), and are markedly larger (48–81%) than those of AOD_{OA} in summer. The reason is that OA reduction rates are decreasing with increasing height both in summer and winter (Figure 6), but at a faster rate in winter due to stable stratification and lower PBLH. In contrast, reduction rates of $PM_{2.5\_SNA}$ are slightly larger than AOD_{SNA} in summer (by up to 8%), but are 1–38% smaller in winter. We find that reduction rates of SNA are decreasing with increasing altitude in summer, but the trend is the opposite in winter below 850 hPa. The model shows that in winter, concentration of NO_3^- is increasing at a faster rate at the surface than aloft. In addition, the ratio of NO_3^-/SNA decreases quickly with increasing height (e.g., NCP in winter: surface: 57%; 750 hPa: 18%). Thus, the resulting total reduction rates of SNA increase with increasing height in winter. The unfavorable chemical processes that buffer NO_3^- reduction in winter have been widely observed and simulated [40,41]. Very few studies have investigated the vertical distribution of $PM_{2.5}$ components in China. The authors in [42] showed that NO_2 is the most important factor that determines the vertical profile of $PM_{2.5}$ in Shanghai in winter. This, in general, explains the important role of NO_3^- on the vertical distribution of $PM_{2.5}$. Observations of vertical profiles of $PM_{2.5}$ components in China are needed in the future to investigate the response of $PM_{2.5}$ components at different altitudes to emission changes.

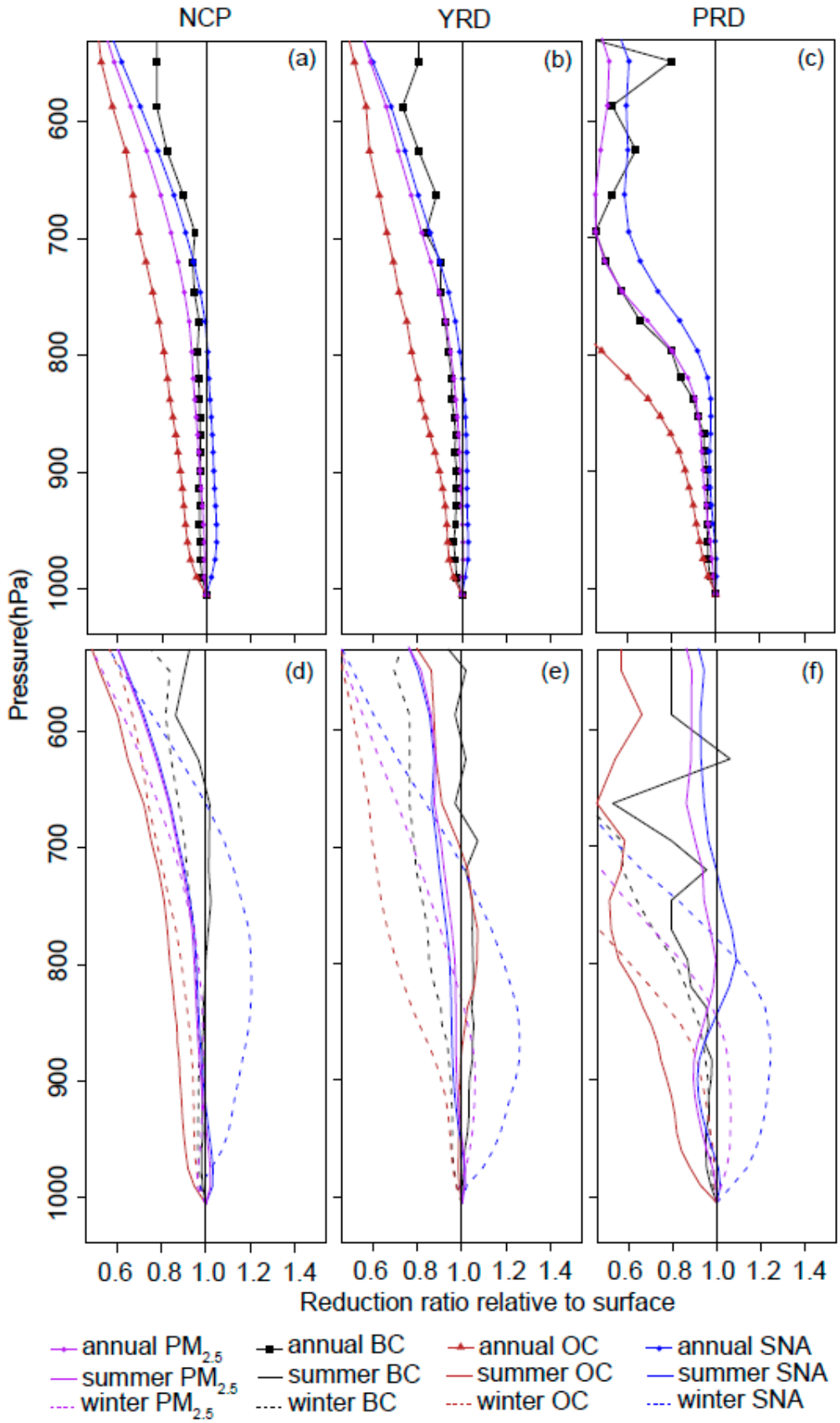

Figure 6. Reduction ratio of $PM_{2.5}$ (($PM_{2.5\_2017}$-$PM_{2.5\_2006}$)/$PM_{2.5\_2006}$, purple) and its components (BC: black lines; OC: brown lines; SNA: blue lines) relative to the surface in 2006–2017 for annual mean (**a**–**c**) and for summer and winter (**d**–**f**) in NCP, YRD and PRD.

3.4. Meteorological Elements That Influence the Correlation of $PM_{2.5}$ and AOD (FIXEMISS)

We estimated the correlation coefficient of $r_{PM\text{-}AOD}$ (correlation coefficient of daily mean $PM_{2.5}$ and AOD in each month in 2006–2017) and monthly mean meteorological elements in each season. The meteorological elements are from MERRA-2 reanalysis data and include temperature (T), an east-west wind component (U), a north-south wind component (V), vertical air movement (O), relative humidity (RH), potential vorticity (PV) at the surface, 850 hPa and 500 hPa, and tropopause pressure (TROPPT), pressure at the surface (PS) and sea level pressure (SLP).

Meteorological elements that have strong correlation with $r_{PM\text{-}AOD}$ vary with regions and seasons (Table 4). T at the surface, 850 hPa and 500 hPa are strongly correlated with $r_{PM\text{-}AOD}$ with correlation coefficients of 0.72–0.88 in NCP and YRD in spring. $T_{surface}$ is also positively related to $r_{PM\text{-}AOD}$ in YRD and PRD in fall, and to $r_{PM\text{-}AOD}$ in PRD in winter. Higher T is usually related to stronger vertical mixing, thus a larger correlation of the surface $PM_{2.5}$ and column AOD.

Table 4. Meteorological elements that have the strongest correlation with $r_{PM\text{-}AOD}$ in NCP, YRD and PRD.

Season	NCP		YRD		PRD	
	Positive	**Negative**	**Positive**	**Negative**	**Positive**	**Negative**
Spring	T_{500hPa} (0.88) $T_{surface}$ (0.84) T_{850hPa} (0.82)	TROPPT (−0.88) PS (−0.77) SLP (−0.67)	T_{500hPa} (0.80) $T_{surface}$ (0.74) T_{850hPa} (0.72)	U_{500hPa} (−0.65) PS (−0.62) SLP (−0.61)	T_{500hPa} (0.80) $dU_{850–500hPa}$ (0.78) RH_{500hPa} (0.77)	U_{500hPa} (−0.82) PS (−0.76) O_{500hPa} (−0.46)
Summer	$dV_{surface–850hPa}$ (0.45) U_{850hPa} (0.43) $dT_{850–500hPa}$ (0.41)	PS (−0.53) SLP (−0.46) V_{500hPa} (−0.38)	V_{500hPa} (0.54) V_{850hPa} (0.42) TROPPT (0.38)	U_{500hPa} (−0.38) $dV_{surface–850hPa}$ (−0.33) PV_{850hPa} (−0.31)	RH_{850hPa} (0.53) RH_{500hPa} (0.42) PV_{850hPa} (0.36)	$dT_{850–500hPa}$ (−0.49) O_{850hPa} (−0.44) SLP (−0.41)
Fall	$dV_{surface–850hPa}$ (0.44) $dT_{850–500hPa}$ (0.37) PBLH (0.33)	PV_{850hPa} (−0.41) RH_{500hPa} (−0.25) SLP (−0.24)	$T_{surface}$ (0.46) T_{850hPa} (0.43) T_{500hPa} (0.39)	$U_{surface}$ (−0.40) U_{500hPa} (−0.38) TROPPT (−0.37)	$T_{surface}$ (0.39) $dU_{850–500hPa}$ (0.38) $dT_{surface–850hPa}$ (0.38)	U_{500hPa} (−0.42) PS (−0.34) SLP (−0.34)
Winter	O_{850hPa} (0.67) $U_{surface}$ (0.60) $dV_{surface–850hPa}$ (0.60)	RH_{850hPa} (−0.54) PREC (−0.51) V_{850hPa} (−0.51)	O_{850hPa} (0.37) O_{500hPa} (0.25) PS (0.24)	RH_{500hPa} (−0.35) PBLH (−0.33) TROPPT (−0.30)	$T_{surface}$ (0.54) $dT_{850–500hPa}$ (0.46) T_{850hPa} (0.45)	PV_{850hPa} (−0.39) $O_{surface}$ (−0.37) U_{500hPa} (−0.34)

Wind in zonal and meridional directions show different correlations with $r_{PM\text{-}AOD}$ in the three regions (Table 4). Zonal wind is positively related to $r_{PM\text{-}AOD}$ in NCP but negatively related to $r_{PM\text{-}AOD}$ in YRD and PRD. Meridional wind is positively related to $r_{PM\text{-}AOD}$ in YRD and negatively related to $r_{PM\text{-}AOD}$ in NCP. The positive or negative correlation coefficients are attributed to the wind direction. For example, U_{500hPa} is positive (from west to east) in the three regions and is consistently negatively related to $r_{PM\text{-}AOD}$ in YRD and PRD. Faster wind at 500 hPa blows aerosols away and decreases the correlation of surface $PM_{2.5}$ and AOD in the column. In contrast, U_{850hPa} in summer and $U_{surface}$ in winter in NCP are negative (from east to west) in 1/3 of the 36 months and are positively related to $r_{PM\text{-}AOD}$ in NCP. We find that O are positively related to $r_{PM\text{-}AOD}$ in NCP and YRD in winter, but negatively related to $r_{PM\text{-}AOD}$ in PRD in summer and winter. In the former two regions, the vertical air movement is upward, thus larger O means stronger mixing and larger $r_{PM\text{-}AOD}$. In PRD, the vertical movement is downward, thus larger O means stronger isolation between the surface and aloft and smaller $r_{PM\text{-}AOD}$.

PS and SLP are negatively related to $r_{PM\text{-}AOD}$ in the three regions in spring, summer and fall (Table 4). Air flows up and together in a low-pressure system, enhancing vertical mixing. Lower PS means stronger mixing and larger $r_{PM\text{-}AOD}$. dT, dV and dU are indicators of atmospheric stability, thus, they are mostly positively related to $r_{PM\text{-}AOD}$ in the three regions.

We investigated the correlation of $r_{PM\text{-}AOD}$ and RH and PBLH in every season. In spring, RH_{500hPa} is positively related to $r_{PM\text{-}AOD}$ in PRD (r = 0.77), but shows weaker relation in NCP and YRD. $RH_{surface}$ and RH_{850hPa} have relatively weaker relations with $r_{PM\text{-}AOD}$ in the three regions. In summer, RH has relatively weaker correlation with $r_{PM\text{-}AOD}$ in NCP and YRD than in PRD. This is in general agreement with observations, which

showed that RH correction increased the $r_{PM\text{-}AOD}$ in the three regions with the largest percentage increase in PRD [15]. PBLH is positively related to $r_{PM\text{-}AOD}$ in NCP ($r = 0.61$), but is relatively weakly related to $r_{PM\text{-}AOD}$ in other seasons and other regions ($-0.33 < r < 0.33$). This is in general agreement with a recent study, which showed that PBLH-PM correlations are stronger in polluted regions than in clean regions [43]. PBLH correction deteriorates the correlation in YRD and PRD in spring [15].

4. Discussion

We use model experiments to separate contributions from anthropogenic emission control and meteorology changes to the $PM_{2.5}$–AOD relationship. We find that η decreased significantly in 2006–2017, due mainly to anthropogenic emission control. With further reduction of anthropogenic emissions in the future, the $PM_{2.5}$–AOD relation is predicted to become weaker. Previous observation-based studies also detected weakening trends of the $PM_{2.5}$–AOD relationship in the last five years [12]. However, it was difficult to investigate reasons for the trends based only on observations.

GEOS-Chem simulation showed that $r_{PM\text{-}AOD}$ showed no statistically significant trends but large inter-annual variations. Meteorological elements are critical in explaining the inter-annual variations of $r_{PM\text{-}AOD}$, such as T, U, V, O, PS, atmospheric instability, RH and PBLH. Among these elements, RH and PBLH were well discussed in previous observation-based studies. Using correction of RH and PBLH improves the correlation of monthly $PM_{2.5}$ and AOD in Beijing in 2011–2015 from 0.63 to 0.76 [9]. The authors in [17] suggested correcting surface $PM_{2.5}$ retrieval using PBLH in northwest China. RH tends to weaken the $r_{PM\text{-}AOD}$ regardless of geographical location [13]. Corrected by RH and PBLH, $r_{PM\text{-}AOD}$ increased in most regions but decreased in a few of the 368 cities in China [15]. $r_{PM\text{-}AOD}$ decreases with increasing surface wind speed [15]. Other meteorological elements were rarely discussed. However, this study shows that T, PS and atmospheric instability are also important to the variations of $r_{PM\text{-}AOD}$, and should be considered in future research.

Despite the strong relation between surface $PM_{2.5}$ and AOD, they show a lot of differences. First, surface $PM_{2.5}$ and AOD show completely different seasonality [22,36]. Second, surface $PM_{2.5}$ and AOD respond differently to emission changes. With the anthropogenic emission changes in 2006–2017, fractional reduction rates of surface $PM_{2.5}$ are larger than AOD. Third, influences of meteorology changes on the inter-annual variation of AOD are larger than that of surface $PM_{2.5}$ [22]. Fourth, despite steady improvement of data quality, uncertainties of AOD values obtained by space-borne remote sensors are so large that they can hardly be used to detect the long-term variations [44]. Even for a global mean quantity, the discrepancies among different products exceed the signal of inter-annual variability [44]. On regional scales, the uncertainties are much larger and more complex. MODIS Terra and Aqua show opposite trends (Terra: -0.009 yr^{-1}; Aqua: $+0.0012$ yr^{-1}) in China in 2001–2011, and both are statistically significant at 95% confidence level [45]. Lastly, studies showed that weaker PM-AOD relationship deteriorate $PM_{2.5}$ retrieval. The authors in [12] showed that adjusted R^2 of $PM_{2.5}$ retrieval decreased from 0.87 in 2013 to 0.69 in 2017 owing to the weakening of the PM-AOD relationship. With the strong reduction of surface $PM_{2.5}$ in recent years and in the future, the $PM_{2.5}$–AOD relationship becomes weaker and the retrieval of $PM_{2.5}$ becomes worse [12]. The predictability of surface $PM_{2.5}$ using space-borne AOD needs further validation.

5. Conclusions

We studied the $PM_{2.5}$–AOD relationship in NCP, YRD and PRD in China using a nested 3D chemical transport model—GEOS-Chem. We separated the contributions from anthropogenic emission control and meteorology changes by fixing meteorology at the 2009 level and fixing anthropogenic emissions at the 2006 level, respectively. We found that η was decreasing in 2006–2017, but $r_{PM\text{-}AOD}$ showed no statistically significant trends. The decrease of η was determined to be caused by anthropogenic emission changes. The vertical distribution of reduction rates varies with seasons and $PM_{2.5}$ components. In summer, all

components reduce slower with increasing height, while in winter the reduction rate of SNA increases first and then decreases. The overall effect of the different trends of different components is that $PM_{2.5}$ concentration decreases slower at higher altitude than at the surface. The inter-annual variations of $r_{PM\text{-}AOD}$ were mainly determined by meteorology changes. We found that major meteorological elements that have strong correlation with $r_{PM\text{-}AOD}$ vary with regions and seasons. T was positively related to $r_{PM\text{-}AOD}$ in the three regions and was particularly important in spring and fall. Horizontal wind speed and vertical air movement show a strong correlation with $r_{PM\text{-}AOD}$. PS is mostly negatively related to $r_{PM\text{-}AOD}$, while atmospheric instability is positively related to $r_{PM\text{-}AOD}$. RH is negatively related to $r_{PM\text{-}AOD}$ in NCP and YRD in fall and winter, but is positively related to $r_{PM\text{-}AOD}$ in PRD in spring and summer. PBLH is positively related to NCP in fall and negatively related to YRD in winter and PRD in spring. This study suggests using other meteorological elements mentioned above when analyzing the $PM_{2.5}$–AOD relationship or retrieving surface $PM_{2.5}$ using satellite AOD. In addition, as the $PM_{2.5}$–AOD relationship weakens with decreasing anthropogenic emissions, validity of remote-sensing surface $PM_{2.5}$ retrieval should be regularly evaluated.

Author Contributions: Conceptualization, L.Q. and S.W.; methodology, L.Q. and D.D.; software, L.Q.; formal analysis, L.Q.; data curation, H.Z. and D.D.; writing—original draft preparation, L.Q.; writing—review and editing, L.Q. and S.W.; funding acquisition, L.Q. and S.W.; supervision, S.W. All authors have read and agreed to the published version of the manuscript.

Funding: This work was funded by the National Natural Science Foundation of China (No. 21806088), Beijing Natural Science Foundation (No. 8222066) and Fundamental Research Funds for the Central Universities (No. FRF-TP-20-056A1).

Data Availability Statement: Data is contained within the article.

Acknowledgments: We thank the support of Samsung Advanced Institute of Technology and National Environmental and Energy Science and Technology International Cooperation Base. S.W. acknowledges the support from the Tencent Foundation through the XPLORER PRIZE. The simulations were completed on the "Explorer 100" cluster system of Tsinghua National Laboratory for Information Science and Technology.

Conflicts of Interest: The authors declare no conflict of interest.

References

1. Liu, J.; Yin, H.; Tang, X.; Zhu, T.; Zhang, Q.; Liu, Z.; Tang, X.; Yi, H. Transition in air pollution, disease burden and health cost in China: A comparative study of long-term and short-term exposure. *Environ. Pollut.* **2021**, *277*, 116770. [CrossRef] [PubMed]
2. Burnett, R.; Chen, H.; Szyszkowicz, M.; Fann, N.; Hubbell, B.; Pope, C.A., 3rd; Apte, J.S.; Brauer, M.; Cohen, A.; Weichenthal, S.; et al. Global estimates of mortality associated with long-term exposure to outdoor fine particulate matter. *Proc. Natl. Acad. Sci. USA* **2018**, *115*, 9592–9597. [CrossRef] [PubMed]
3. Xue, T.; Zheng, Y.; Tong, D.; Zheng, B.; Li, X.; Zhu, T.; Zhang, Q. Spatiotemporal continuous estimates of PM2.5 concentrations in China, 2000–2016: A machine learning method with inputs from satellites, chemical transport model, and ground observations. *Environ. Int.* **2019**, *123*, 345–357. [CrossRef] [PubMed]
4. Geng, G.; Zhang, Q.; Martin, R.V.; van Donkelaar, A.; Huo, H.; Che, H.; Lin, J.; He, K. Estimating long-term PM2.5 concentrations in China using satellite-based aerosol optical depth and a chemical transport model. *Remote Sens. Environ.* **2015**, *166*, 262–270. [CrossRef]
5. Zheng, Y.; Zhang, Q.; Liu, Y.; Geng, G.; He, K. Estimating ground-level PM2.5 concentrations over three megalopolises in China using satellite-derived aerosol optical depth measurements. *Atmos. Environ.* **2016**, *124*, 232–242. [CrossRef]
6. He, Q.; Gu, Y.; Zhang, M. Spatiotemporal trends of PM2.5 concentrations in central China from 2003 to 2018 based on MAIAC-derived high-resolution data. *Environ. Int.* **2020**, *137*, 105536. [CrossRef]
7. Xin, J.; Gong, C.; Liu, Z.; Cong, Z.; Gao, W.; Song, T.; Pan, Y.; Sun, Y.; Ji, D.; Wang, L.; et al. The observation-based relationships between PM2.5and AOD over China. *J. Geophys. Res. Atmos.* **2016**, *121*, 10701–10716. [CrossRef]
8. Wang, J. Intercomparison between satellite-derived aerosol optical thickness and PM2.5mass: Implications for air quality studies. *Geophys. Res. Lett.* **2003**, *30*, 2095. [CrossRef]
9. Zheng, C.; Zhao, C.; Zhu, Y.; Wang, Y.; Shi, X.; Wu, X.; Chen, T.; Wu, F.; Qiu, Y. Analysis of influential factors for the relationship between PM2.5 and AOD in Beijing. *Atmos. Chem. Phys.* **2017**, *17*, 13473–13489. [CrossRef]

10. Kong, L.; Xin, J.; Zhang, W.; Wang, Y. The empirical correlations between PM2.5, PM10 and AOD in the Beijing metropolitan region and the PM2.5, PM10 distributions retrieved by MODIS. *Environ. Pollut.* **2016**, *216*, 350–360. [CrossRef]
11. Shao, P.; Xin, J.; An, J.; Kong, L.; Wang, B.; Wang, J.; Wang, Y.; Wu, D. The empirical relationship between PM2.5 and AOD in Nanjing of the Yangtze River Delta. *Atmos. Pollut. Res.* **2017**, *8*, 233–243. [CrossRef]
12. Yang, Q.; Yuan, Q.; Yue, L.; Li, T.; Shen, H.; Zhang, L. The relationships between PM2.5 and aerosol optical depth (AOD) in mainland China: About and behind the spatio-temporal variations. *Environ. Pollut.* **2019**, *248*, 526–535. [CrossRef] [PubMed]
13. Guo, J.; Xia, F.; Zhang, Y.; Liu, H.; Li, J.; Lou, M.; He, J.; Yan, Y.; Wang, F.; Min, M.; et al. Impact of diurnal variability and meteorological factors on the PM2.5—AOD relationship: Implications for PM2.5 remote sensing. *Environ. Pollut.* **2017**, *221*, 94–104. [CrossRef] [PubMed]
14. Xu, Q.; Chen, X.; Yang, S.; Tang, L.; Dong, J. Spatiotemporal relationship between Himawari-8 hourly columnar aerosol optical depth (AOD) and ground-level PM2.5 mass concentration in mainland China. *Sci. Total Environ.* **2021**, *765*, 144241. [CrossRef]
15. He, Q.; Wang, M.; Yim, S.H.L. The spatiotemporal relationship between PM2.5 and aerosol optical depth in China: Influencing factors and implications for satellite PM2.5 estimations using MAIAC aerosol optical depth. *Atmos. Chem. Phys.* **2021**, *21*, 18375–18391. [CrossRef]
16. Wang, Z.; Chen, L.; Tao, J.; Liu, Y.; Hu, X.; Tao, M. An empirical method of RH correction for satellite estimation of ground-level PM concentrations. *Atmos. Environ.* **2014**, *95*, 71–81. [CrossRef]
17. Gong, W.; Huang, Y.; Zhang, T.; Zhu, Z.; Ji, Y.; Xiang, H. Impact and Suggestion of Column-to-Surface Vertical Correction Scheme on the Relationship between Satellite AOD and Ground-Level PM2.5 in China. *Remote Sens.* **2017**, *9*, 1038. [CrossRef]
18. Li, M.; Liu, H.; Geng, G.; Hong, C.; Liu, F.; Song, Y.; Tong, D.; Zheng, B.; Cui, H.; Man, H.; et al. Anthropogenic emission inventories in China: A review. *Natl. Sci. Rev.* **2017**, *4*, 834–866. [CrossRef]
19. Yin, L.; Du, P.; Zhang, M.; Liu, M.; Xu, T.; Song, Y. Estimation of emissions from biomass burning in China (2003–2017) based on MODIS fire radiative energy data. *Biogeosciences* **2019**, *16*, 1629–1640. [CrossRef]
20. Bilal, M.; Nazeer, M.; Nichol, J.; Qiu, Z.; Wang, L.; Bleiweiss, M.; Shen, X.; Campbell, J.; Lolli, S. Evaluation of Terra-MODIS C6 and C6.1 Aerosol Products against Beijing, XiangHe, and Xinglong AERONET Sites in China during 2004–2014. *Remote Sens.* **2019**, *11*, 486. [CrossRef]
21. He, Q.; Li, C.; Tang, X.; Li, H.; Geng, F.; Wu, Y. Validation of MODIS derived aerosol optical depth over the Yangtze River Delta in China. *Remote Sens. Environ.* **2010**, *114*, 1649–1661. [CrossRef]
22. Qi, L.; Zheng, H.; Ding, D.; Ye, D.; Wang, S. Effects of Meteorology Changes on Inter-Annual Variations of Aerosol Optical Depth and Surface PM2.5 in China—Implications for PM2.5 Remote Sensing. *Remote Sens.* **2022**, *14*, 2762. [CrossRef]
23. Booker, D.H.R.M.J. *UK Equivalence Programme for Monitoring of Particulate Matter*; BV/AQ/AD202209/DH/2396; Bureau Veritas: Neuilly-sur-Seine, France, 2006.
24. Song, S.; Gao, M.; Xu, W.; Shao, J.; Shi, G.; Wang, S.; Wang, Y.; Sun, Y.; McElroy, M.B. Fine-particle pH for Beijing winter haze as inferred from different thermodynamic equilibrium models. *Atmos. Chem. Phys.* **2018**, *18*, 7423–7438. [CrossRef]
25. Park, R.J.; Jacob, D.J.; Field, B.D.; Yantosca, R.M.; Chin, M. Natural and transboundary pollution influences on sulfate-nitrate-ammonium aerosols in the United States: Implications for policy. *J. Geophys. Res. Atmos.* **2004**, *109*, D15204. [CrossRef]
26. Alexander, B.; Park, R.J.; Jacob, D.J.; Gong, S. Transition metal-catalyzed oxidation of atmospheric sulfur: Global implications for the sulfur budget. *J. Geophys. Res.* **2009**, *114*, D02309. [CrossRef]
27. Pye, H.O.T.; Chan, A.W.H.; Barkley, M.P.; Seinfeld, J.H. Global modeling of organic aerosol: The importance of reactive nitrogen (NO_x and NO_3). *Atmos. Chem. Phys.* **2010**, *10*, 11261–11276. [CrossRef]
28. Marais, E.A.; Jacob, D.J.; Jimenez, J.L.; Campuzano-Jost, P.; Day, D.A.; Hu, W.; Krechmer, J.; Zhu, L.; Kim, P.S.; Miller, C.C.; et al. Aqueous-phase mechanism for secondary organic aerosol formation from isoprene: Application to the Southeast United States and co-benefit of SO_2 emission controls. *Atmos. Chem. Phys.* **2016**, *16*, 1603–1618. [CrossRef]
29. Fairlie, T.D.; Jacob, D.J.; Dibb, J.E.; Alexander, B.; Avery, M.A.; van Donkelaar, A.; Zhang, L. Impact of mineral dust on nitrate, sulfate, and ozone in transpacific Asian pollution plumes. *Atmos. Chem. Phys.* **2010**, *10*, 3999–4012. [CrossRef]
30. Zheng, H.; Zhao, B.; Wang, S.; Wang, T.; Ding, D.; Chang, X.; Liu, K.; Xing, J.; Dong, Z.; Aunan, K.; et al. Transition in source contributions of PM2.5 exposure and associated premature mortality in China during 2005–2015. *Environ. Int.* **2019**, *132*, 105111. [CrossRef]
31. Randerson, J.T.; Van Der Werf, G.R.; Giglio, L.; Collatz, G.J.; Kasibhatla, P.S. *Global Fire Emissions Database, Version 4.1 (GFEDv4)*; ORNL DAAC: Oak Ridge, TN, USA, 2018. [CrossRef]
32. Zhang, L.; Gong, S.; Padro, J.; Barrie, L. A size-segregated particle dry deposition scheme for an atmospheric aerosol module. *Atmos. Environ.* **2001**, *35*, 549–560. [CrossRef]
33. Wang, Q.; Jacob, D.J.; Spackman, J.R.; Perring, A.E.; Schwarz, J.P.; Moteki, N.; Marais, E.A.; Ge, C.; Wang, J.; Barrett, S.R.H. Global budget and radiative forcing of black carbon aerosol: Constraints from pole-to-pole (HIPPO) observations across the Pacific. *J. Geophys. Res.-Atmos.* **2014**, *119*, 195–206. [CrossRef]
34. Miao, R.; Chen, Q.; Zheng, Y.; Cheng, X.; Sun, Y.; Palmer, P.I.; Shrivastava, M.; Guo, J.; Zhang, Q.; Liu, Y.; et al. Model bias in simulating major chemical components of PM2.5 in China. *Atmos. Chem. Phys.* **2020**, *20*, 12265–12284. [CrossRef]
35. Ma, Z.; Liu, R.; Liu, Y.; Bi, J. Effects of air pollution control policies on PM2.5 pollution improvement in China from 2005 to 2017: A satellite-based perspective. *Atmos. Chem. Phys.* **2019**, *19*, 6861–6877. [CrossRef]

36. Xu, J.; Han, F.; Li, M.; Zhang, Z.; Xiaohui, D.; Wei, P. On the opposite seasonality of MODIS AOD and surface PM2.5 over the Northern China plain. *Atmos. Environ.* **2019**, *215*, 116909. [CrossRef]
37. Van Donkelaar, A.; Martin, R.V.; Brauer, M.; Kahn, R.; Levy, R.; Verduzco, C.; Villeneuve, P.J. Global estimates of ambient fine particulate matter concentrations from satellite-based aerosol optical depth: Development and application. *Environ. Health Perspect.* **2010**, *118*, 847–855. [CrossRef]
38. Zhang, Q.; Zheng, Y.; Tong, D.; Shao, M.; Wang, S.; Zhang, Y.; Xu, X.; Wang, J.; He, H.; Liu, W.; et al. Drivers of improved PM2.5 air quality in China from 2013 to 2017. *Proc. Natl. Acad. Sci. USA* **2019**, *116*, 24463–24469. [CrossRef]
39. Ma, Q.; Zhang, Q.; Wang, Q.; Yuan, X.; Yuan, R.; Luo, C. A comparative study of EOF and NMF analysis on downward trend of AOD over China from 2011 to 2019. *Environ. Pollut.* **2021**, *288*, 117713. [CrossRef]
40. Leung, D.M.; Shi, H.; Zhao, B.; Wang, J.; Ding, E.M.; Gu, Y.; Zheng, H.; Chen, G.; Liou, K.N.; Wang, S. Wintertime particulate matter decrease buffered by unfavorable chemical processes despite emissions reductions in China. *Geophys. Res. Lett.* **2020**, *47*, e2020GL087721. [CrossRef]
41. Shah, V.; Jaeglé, L.; Thornton, J.A.; Lopez-Hilfiker, F.D.; Lee, B.H.; Schroder, J.C.; Campuzano-Jost, P.; Jimenez, J.L.; Guo, H.; Sullivan, A.P.; et al. Chemical feedbacks weaken the wintertime response of particulate sulfate and nitrate to emissions reductions over the eastern United States. *Proc. Natl. Acad. Sci. USA* **2018**, *115*, 8110–8115. [CrossRef]
42. Zhang, K.; Zhou, L.; Fu, Q.; Yan, L.; Morawska, L.; Jayaratne, R.; Xiu, G. Sources and vertical distribution of PM2. 5 over Shanghai during the winter of 2017. *Sci. Total Environ.* **2020**, *706*, 135683. [CrossRef]
43. Su, T.; Li, Z.; Kahn, R. Relationships between the planetary boundary layer height and surface pollutants derived from lidar observations over China: Regional pattern and influencing factors. *Atmos. Chem. Phys.* **2018**, *18*, 15921–15935. [CrossRef]
44. Li, Z.; Zhao, X.; Kahn, R.; Mishchenko, M.; Remer, L.; Lee, K.; Wang, M.; Laszlo, I.; Nakajima, T.; Maring, H. Uncertainties in satellite remote sensing of aerosols and impact on monitoring its long-term trend: A review and perspective. *Ann. Geophys.* **2009**, *27*, 2755–2770. [CrossRef]
45. Cheng, T.; Chen, H.; Gu, X.; Yu, T.; Guo, J.; Guo, H. The inter-comparison of MODIS, MISR and GOCART aerosol products against AERONET data over China. *J. Quant. Spectrosc. Radiat. Transf.* **2012**, *113*, 2135–2145. [CrossRef]